Supporting Information for

Heterogeneous single-sites synergetic catalysis for spontaneous photocatalytic overall water splitting

Hui Su, Meihuan Liu, Weiren Cheng*, Xu Zhao, Fengchun Hu, and Qinghua Liu*

National Synchrotron Radiation Laboratory, University of Science and Technology of China, Hefei 230029, Anhui, P. R. China

S1. Materials

Pt-Au/C_3N_4 preparation: graphitic carbon nitride (g-C_3N_4) was prepared by the commonly used thermal polymerization of urea at 550 °C for 4 h and then was treated by 38 vol% ammonia solution maintaining at 80 °C for 6 h to obtain ammonia-treatment g-C_3N_4. Subsequently, 120 mg ammonia-treatment g-C_3N_4 was ultrasonic dispersion in 100 mL deionized water and then 0.50 mL $HAuCl_4 \cdot 4H_2O$ (29.5 mM) and 0.45 mL $H_2PtCl_6 \cdot 6H_2O$ (20 mM) were added dropwise into the suspension under vigorous stirring. After that, the resultant solution was continuously stirred at room temperature (25 °C) for 8 h and then was centrifuged, washed, and dried at 60 °C overnight to gain the pale yellow powder noted as Pt-Au/C_3N_4. The Pt/C_3N_4 or Au/C_3N_4 was synthesized in the similar process mentioned above without addition of $HAuCl_4 \cdot 4H_2O$ or $H_2PtCl_6 \cdot 6H_2O$, respectively.

S2. Materials characterization

Transmission electron microscopy (TEM) was performed on a JEM-2100F microscope at an acceleration voltage of 200 kV. Aberration-corrected high angle annular dark field transmission electron microscopy (HAADF-TEM) was conducted on a JEM-ARM200F instrument at 200 kV. The X-ray diffraction (XRD) patterns were performed on Philips X'Pert Pro Super X-ray diffractometer with Cu *Kα* radiation. The UV-vis spectra (DRS) were recorded on a Shimadzu DUV-3700 spectrophotometer. X-ray photoelectron spectra (XPS) were acquired at the photoemission end-station at beamline BL10B in the National Synchrotron Radiation Laboratory (NSRL) in Hefei, China. The beamline is connected to an undulator and

equipped with two gratings that offer soft X-rays from 100 to 1000 eV with a typical photon flux of 5×10^{10} photons/s and a resolution ($E/\Delta E$) better than 10^3 at 244 eV. The binding energies obtained in the XPS spectral analysis were corrected for specimen charging by referencing C 1s to 284.5 eV.

XAFS measurements. The XAFS data were collected at BL14W1 station in SSRF (Shanghai Synchrotron Radiation Facility) and 1W1B station in BSRF (Beijing Synchrotron Radiation Facility). The storage rings of SSRF and BSRF were operated at 3.5 GeV with the current of 300 mA and at 2.5 GeV with a maximum current of 250 mA, respectively. The acquired EXAFS data were processed according to the standard procedures using the ATHENA module implemented in the IFEFFIT software packages. The k^3-weighted EXAFS spectra were obtained by subtracting the post-edge background from the overall absorption and then normalizing with respect to the edge-jump step. Subsequently, k^3-weighted χ(k) data in the k-space ranging from 2.4–10 $Å^{-1}$ were Fourier transformed to real (R) space using a hanning windows (dk = 1.0 $Å^{-1}$) to separate the EXAFS contributions from different coordination shells.

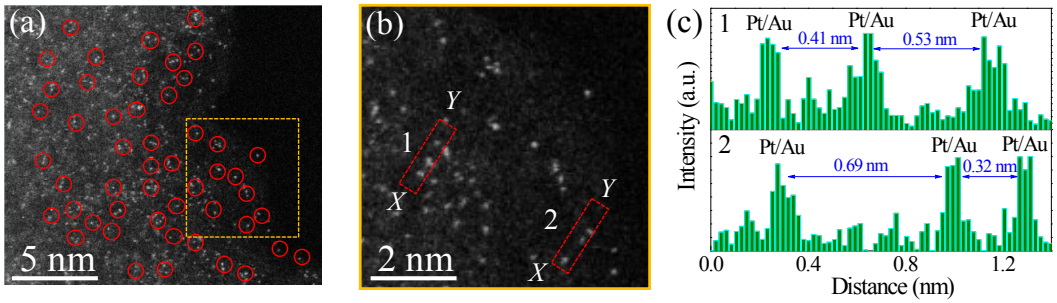

Figure S1. (a) HAADF-TEM images, (b) Magnified HAADF-STEM image and (c) intensity profile along the line *X*-*Y* in the HAADF-STEM image for Pt-Au/C_3N_4.

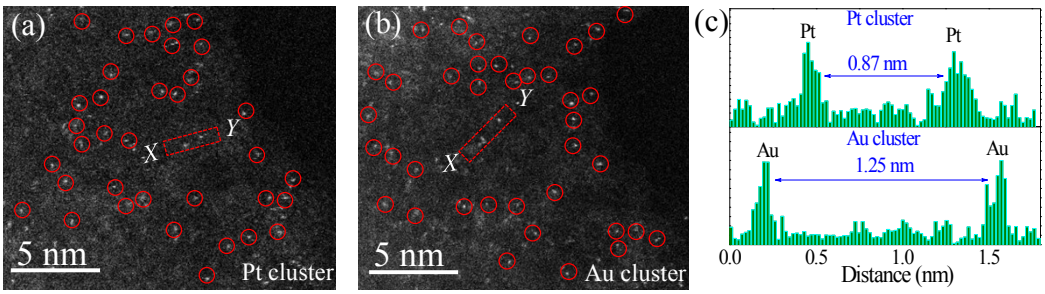

Figure S2. Representative HAADF-STEM for Pt (a) and Au (b) single-site/C_3N_4 and (c)

intensity profiles along the line *X*-*Y* in the HAADF-STEM images.

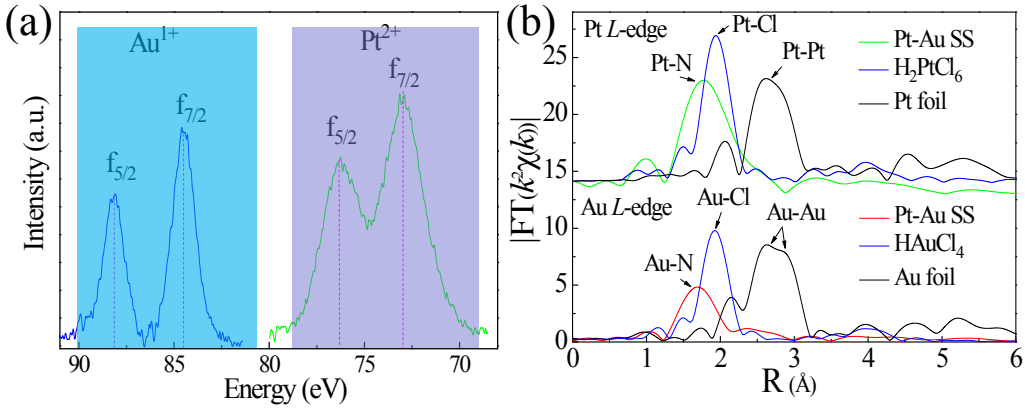

Figure S3. (a) XPS spectra and (b) FT curves of Pt and Au L_3-edge EXAFS oscillations for single-site Pt-Au/C_3N_4.

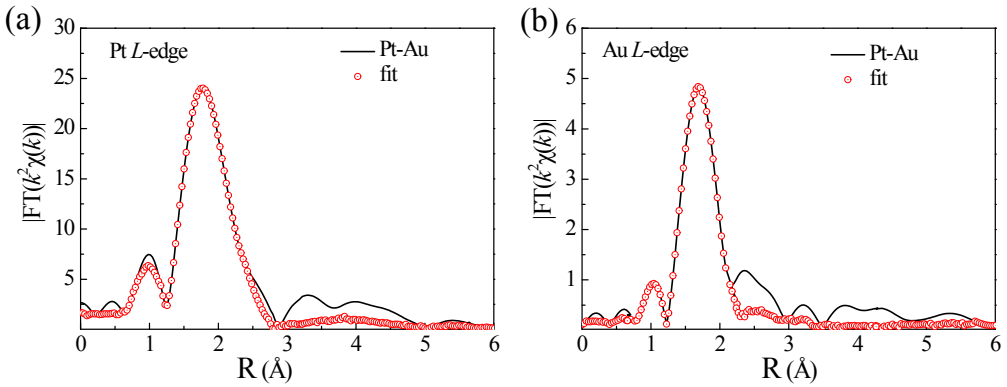

Figure S4. The fitting curve of k^3-weighted EXAFS spectras of Pt *L*-edge (a) and Au *L*-edge for Pt-Au/C_3N_4.

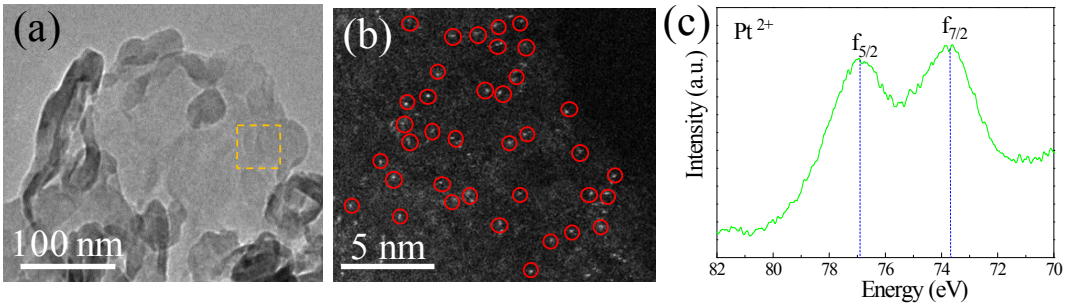

Figure S5. (a) TEM, (b) HAADF-TEM images, and (c) XPS spectra for Pt/C_3N_4.

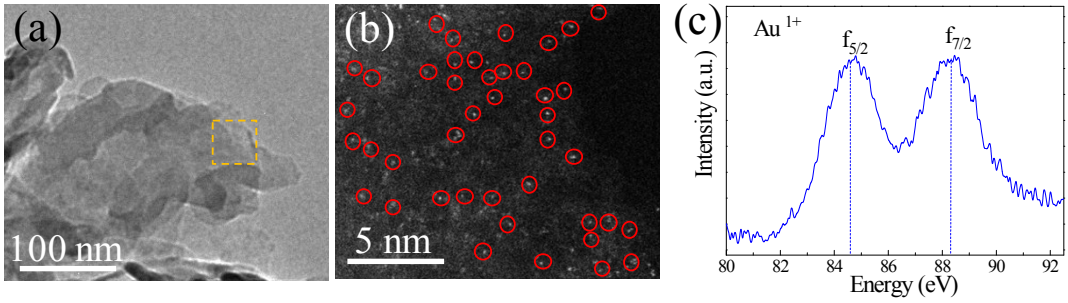

Figure S6. (a) TEM, (b) HAADF-TEM images, and (c) XPS spectra for Au/C_3N_4.

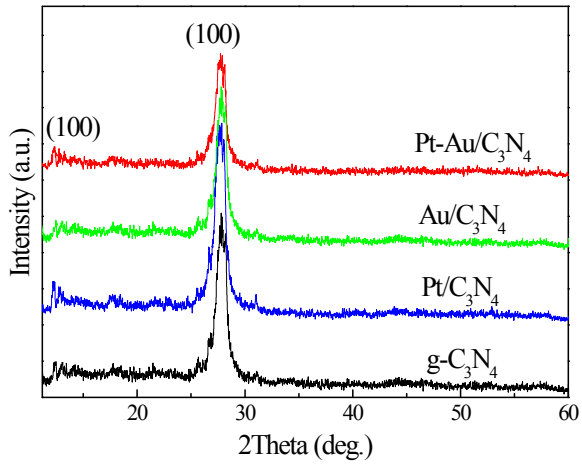

Figure S7. XRD patterns for $g\text{-}C_3N_4$, Pt/C_3N_4, Au/C_3N_4, and $Pt\text{-}Au/C_3N_4$.

Electrochemical measurement methods. Electrochemical measurements were performed using an electrochemical workstation (Model CHI760D, CH instruments, Inc., Austin, TX) with a standard three-electrode photoelectrochemical cell and was used to record redox activity of the samples, where the prepared electrodes immersed in a sodium sulfate electrolyte solution (0.5 M), a gauze platinum and Ag/AgCl (saturated KCl) act as the working, auxiliary, and reference electrode, respectively. The working electrodes were prepared as follows: 5 mg photocatalyst was ground with 5 uL nafion (5 wt%, Sigma Aldrich) and mixed with 2 mL of ethanol under sonication for 30 min to obtain slurry. Then, the slurry was coated onto glassy carbon electrode by the spin coater. In addition, the three electrodes were immersed in a sodium sulfate electrolyte solution (0.5 M) as conductive media at pH 6.8, which was continuously in an N_2-purged flow to remove O_2 before light irradiation.

Photocatalytic reactions and measurements. Photocatalytic hydrogen evolution

performance measurements were carried out in a top-irradiation-type photoreactor (Pyrex glass) connected to a closed gas circulation system. Approximately 30 mg of the photocatalysts were dispersed in 100 ml DI-water. The reactant solution was evacuated several times to remove air thoroughly and irradiated using a 300 W Xe-lamp (PLS-SXE 300, Beijing perfectlight Co. Ltd, China) as the light source. The generated gases were measured by a gas chromatograph (GC) equipped with a thermal conduction detector (TCD, 5 Å molecular sieve columns with 3 m length) using Ar as carrier gas with flow rate of 20 ml/min. The injection port, column, and detector temperatures are 60, 60, and 130 °C, respectively. The 60 cycles with time interval of 6 hours were performed for the samples.

For full spectrum measurement, a 300 W xenon arc lamp (PLS-SXE300/300UV) with a standard AM1.5 filter, outputting the light density of 100 mW/cm^2, was used as illumination source to trigger the photocatalytic reaction for the samples. A series of band-pass filters (FWHM=15 nm) within the UV-visible light region were employed to achieve a different incident light wavelength under a 300 W Xe lamp for measurement of the photocatalytic activity and quantum efficiency. The average intensity of each irradiation wavelength was determined by an optical power meter (PM100D, Thermal Powermeter Head, THORLABS).

The charge separation (C-S) efficiency was determined by using H_2O_2 as the hole scavenger at different irradiation wavelength. Previous studies have shown that H_2O_2 can be used as a hole scavenger to harvest photo-excited holes with nearly 100% efficiency on hematite and TiO_2 semiconductor photocatalysts.[1,2] So it is possible to estimate the C-S efficiency via dividing the H_2 evolution amount measured with H_2O_2 by the number of absorption photons when assuming the absolute absorption of incident photons by photocatalysts. The electron-hole efficiency can be calculated by the equation:

electron-hole efficiency =

$$\frac{2 * the\ number\ of\ evolved\ H2\ molecules\ with\ H2O2}{the\ number\ of\ incident\ photons} \times 100\%.$$

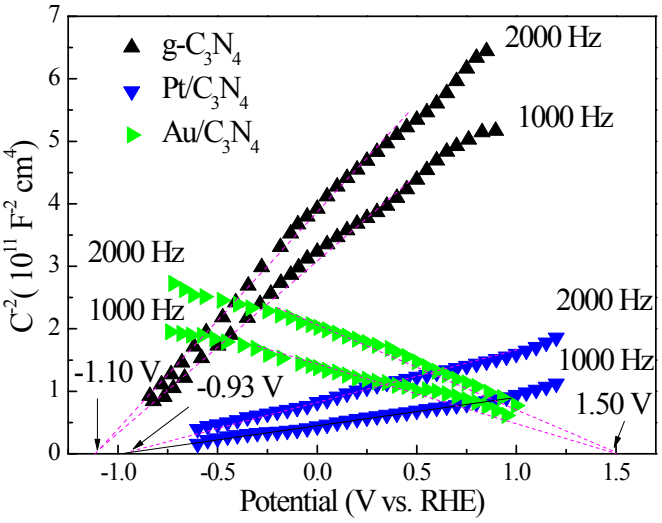

Figure S8. Mott-Schottky plots for g-C_3N_4, Pt/C_3N_4, and Au/C_3N_4.

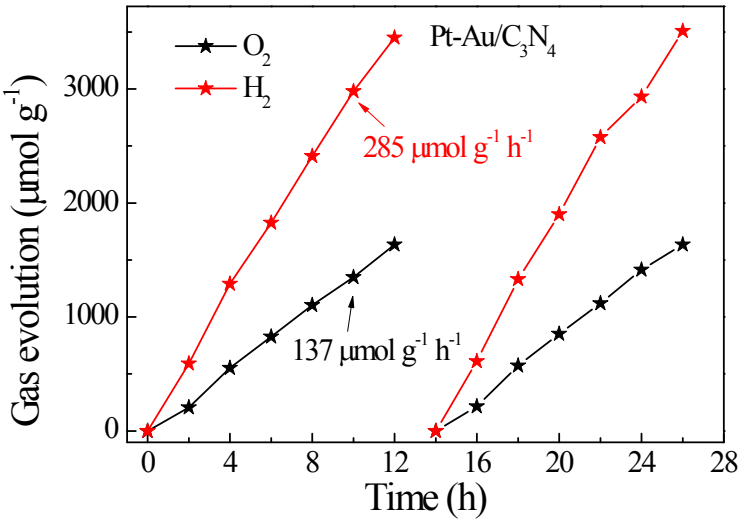

Figure S9. Typical time courses of H_2 and O_2 evolution of Pt-Au/C_3N_4.

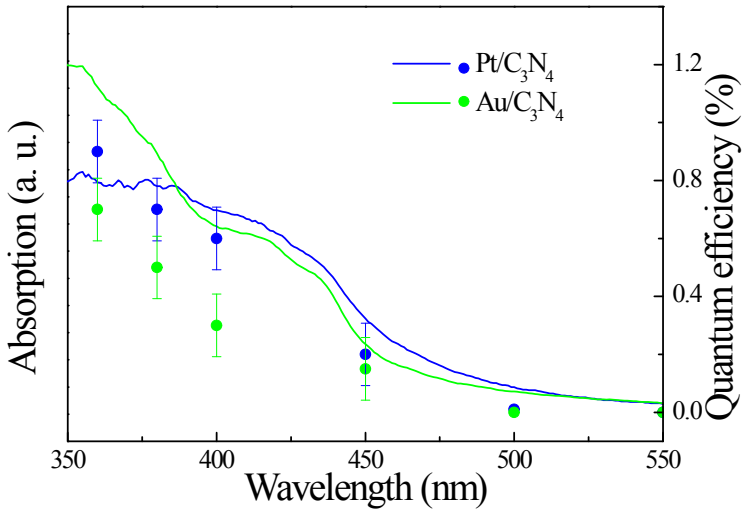

Figure S10. Quantum efficiency for Pt/C_3N_4 and Au/C_3N_4.

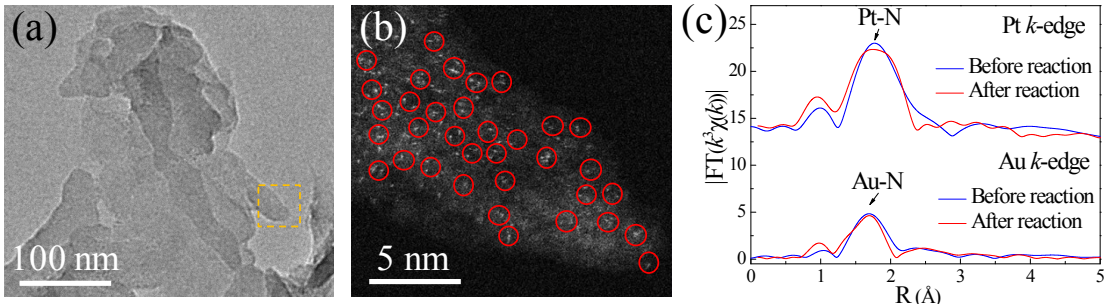

Figure S11. (a) TEM image, (b) HAADF-TEM image, and (c) FT curves of Pt and Au *K*-edge EXAFS functions for the $Pt\text{-}Au/C_3N_4$ after photocatalytic measurement.

Table S1. Fitting parameters for the EIS data of samples.

	g-C_3N_4	**Au/C_3N_4**	**Pt/C_3N_4**	**$Pt\text{-}Au/C_3N_4$**
R_s /Ω	6.3	5.2	4.6	3.2
R_{ct} /Ω	2730	710	504	193
CPE_{int} /mF	0.023	0.69	0.86	0.056
CPE_{DL}/mF	0.0012	0.032	0.067	0.26

Table S2. The EXAFS fitting parameters of Pt-Au/C_3N_4.

Sample	Path	N	R(Å)	$\sigma^2(10^{-3}Å)$	ΔE(eV)
Pt sites for Pt-Au	Pt-N Pt-N	2.0(±0.1) 1.9(±0.1)	2.01(±0.01) 2.08(±0.02)	5(±0.2)	3.5(±0.2)
Au sites for Pt-Au	Au-N	1.9(±0.1)	2.05(±0.01)	6(±0.3)	3.7(±0.2)

Table S3. Comparison of overall water splitting performances with other g-C3N4-based photocatalysts reported in literatures

Photocatalyst	Aqueous electrolyte(PH)	Illumination	H_2, μmol h^{-1} g_{cat}^{-1}	O_2, μmol h^{-1} g_{cat}^{-1}	Quantum yield,(wavelength) efficiency	Ref.
Pt/PtO_2/CoO_X/C_3N_4	Pure water	300 W Xe lamp (>420 nm)	61	31.5	0.3% (405 nm)	3
BD-C_3N_4	Pure water (Pt cocatalyst)	300 W Xe lamp (>450 nm)	1400	702	1.6% (450nm)	4
α-Fe_2O_3/2D-C_3N_4	Pure water (3wt.%Pt/2D -C_3N_4,3wt.% RuO_2/Fe_2O_3)	300 W Xe lamp (>400 nm)	38.2	19.1	--	5
g-C_3N_4-rGO-WO_3	Pure water (1 wt. % Pt)	250 w iron doped metal halide UV-Vis lamp,λ> 420 nm	8.75	4.37	0.9% (420nm)	6
CQDs/g-C_3N_4	Pure water	300 W Xe lamp (>420 nm)	105	51.25	16% (420nm)	7
g-C_3N_4 Nanowire Bundles	Pure water (1 wt.% Pt)	300 W Xe lamp (>420 nm)	72	35.6	5.2% (420nm)	8
Pt-CoP/g-C_3N_4	Pure water (pH=3)	300 W Xe lamp (>420 nm)	26.25	12.50	--	9
Mn-doped Fe_2O_3/ g-C_3N_4	Pure water (1 wt.% Pt)	300 W Xe lamp (>400 nm)	51μmol h^{-1}	25μmol h^{-1}	--	10
Pt/$Ni(OH)_2$-C_3N_4	Pure water	300 W Xe lamp	425.7	201.2	1.8%(420 nm)	11
Pt/C_3N_4	Pure water	300 W Xe lamp	40	--	0.4% (420 nm)	This work
Au/C_3N_4	Pure water	300 W Xe lamp	28	--	0.2% (420nm)	This work
Pt-Au cluster/C_3N_4	Pure water	300 W Xe lamp	285	142	3% (420nm)	This work

S3. DFT calculation details

The first-principles density functional theory (DFT) calculations were performed using a plane wave basis set with the projector augmented plane-wave (PAW) method.[3,4] The exchange-correlation interaction was described within the generalized gradient approximation (GGA) in the form of PW91.[5] The energy cutoff was set to

400 eV, and the atomic positions were allowed to relax until the energy and force were less than 10^{-4} eV and 10^{-2} eV/Å, respectively. The graphitic carbon nitride was modeled in supercell geometry containing up to four tri-s-triazine units and the graphitic planes were separated by a vacuum region of 15 Å.

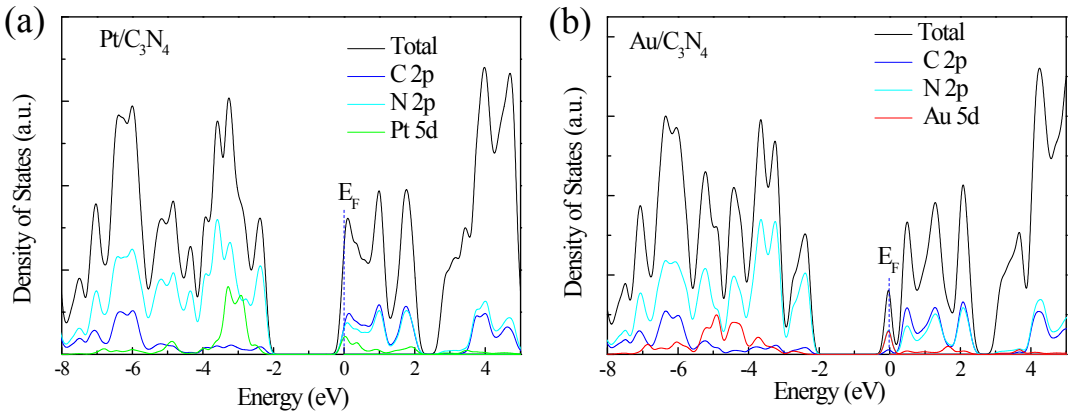

Figure S12. DOS plots for Pt/C_3N_4 and Au/C_3N_4.

References

[1] Dotan, H.; Sivula, K.; Gratzel, M.; Rothschild, A.; Warren, S. C. *Energy Environ. Sci.* **2011**, *4 (3)*, 958−964.

[2] Wang, G.; Xiao, X.; Li, W.; Lin, Z.; Zhao, Z.; Chen, C.; Wang, C.; Li, Y.; Huang, X.; Miao, L.; Jiang, C.; Huang, Y.; Duan, X. *Nano letters* **2015**, *15*, 4692.

[3] Zhang, G.; Lan, Z.-A.; Lin, L.; Lin, S.; Wang, X. *Chem. Sci.* **2016**, *7*, 3062-3066.

[4] Bellamkonda, S.; Shanmugam, R.; Gangavarapu, r. r.; *J. Mater. Chem. A*, **2019**, *7*, 3757-3771.

[5] She, X.; Wu, J.; Xu, H.; Zhong, J.; Wang, Y.; Song, Y.; Nie, K.; Liu, Y.; Yang, Y.; Rodrigues, M. T. F.; Vajtai, R.; Lou, J.; Du, D.; Li, H.; Ajayan, P. M. *Adv. Energy Mater.*, **2017**, 7, 1700025

[6] Zhao, G.; Huang, X.; Fina, F.; Zhang, G.; Irvine, J. T. S. *Catal. Sci. Techno.* 2015, 5, 3416-3422.

[7] Liu, j.; Liu, Y.; Liu, n.; Han, Y.; Zhang, X.; Huang, H.; Lifshitz, Y.; Lee, s. t.; Zhong, J.; Kang, Z. *Science.* **2015,** *347*, 970-974

[8] Zhang, K.; Wang, L.; Sheng, X.; Ma, M.; Jung, M. S.; Kin, W.; Lee, H.; Park, J. H. *Adv. Energy Mater.* **2016,** *6*, 1502352
[9] Pan, Z.; Zheng, Y.; Guo, F.; Niu, P.; Wang, X. *ChemSusChem.* **2017,** *10*, 87-90.
[10] Wang, N., Han, B.; Wen, J.; Liu, M.; Li, X. *Colloids and Surfaces A* **2019**, 567, 313–318
[11] Sun, S.; Zhang, Y. C.; Shen, G.; Wang, Y.; Liu, X.; Duan, Z.; Pan, L.; Zhang, X.; Zou, J. J. *Appl. Catal. B-Environ.* **2019**, 243, 253–261
[12] Samanta, S.; Martha, S.; Parida, K. *ChemCatChem,* **2014***, 6,* 1453-1462.
[13] Jiang J.; Yu, J.; Cao, S. W. J. *Colloid interf. Sci.* **2016***, 461*, 56-63.
[14] Furthmiiller, G. K. J. *Computufional Murerials Scienc***e 1996***, 6*, 15.